



A study on the active sites for visible-light photocatalytic activity of phosphorus-doped titanium(IV) oxide particles prepared using a phosphide compound

Motoki Iwase^a, Keiji Yamada^a, Tsutomu Kurisaki^a, Bunsho Ohtani^b, Hisanobu Wakita^{a,*}

^a Department of Chemistry, Faculty of Science, Fukuoka University, 8-19-1 Nanakuma, Jonan-ku, Fukuoka 814-0180, Japan

^b Catalysis Research Center, Hokkaido University, Sapporo 001-0021, Japan

ARTICLE INFO

Article history:

Received 8 February 2013

Received in revised form 1 April 2013

Accepted 7 April 2013

Available online 13 April 2013

Keywords:

Titania

Phosphorus

Photocatalysis

Phosphorus-doped titania

Phosphide

ABSTRACT

The properties of a series of negatively-charged phosphorus (P)-doped titanium(IV) oxide (TiO₂) particles were investigated for their dependence on P concentration. XRD peak broadening demonstrated that the crystallite sizes of the P-doped TiO₂ particles decreased with increasing P concentration, suggesting that P atom dopants inhibit crystalline growth. The P-doped TiO₂ nanoparticles exhibited a pale yellow color. The UV–vis diffuse reflection spectra of the P-doped TiO₂ nanoparticles demonstrated a continuous and tailing absorption in the visible region. The broad absorption band in the range of 500–600 nm increased with increasing P content, presumably due to an increase in the density of oxygen vacancies. However, the increase in the density of the oxygen vacancies did not correspond to the change of phenol degradation rate under visible-light irradiation. The results suggest that the oxygen vacancies in P-doped TiO₂ are inactive to visible light.

© 2013 Elsevier B.V. All rights reserved.

1. Introduction

Titanium(IV) oxide (TiO₂), especially anatase powder, has been recognized as one of the most promising materials for the remediation of environmental organic pollutants because of the advantage of being a nontoxic, stable and inexpensive photocatalyst [1–3]. However, excitation of anatase TiO₂ requires light of energy greater than 3.2 eV, i.e., ultraviolet light, which comprises only ~6% of solar radiation. A great deal of effort has been performed to reduce the band-gap energy of TiO₂ by doping the nanoparticles with transition metal cations [4,5] and non-metal anions of elements such as nitrogen [6–16], carbon [17,18] and sulfur [19,20]. Some examples of precursor substances that were used to prepare N-doped TiO₂ were ammonia [6–9], urea [10–12], ethylenediamine [13], ethylmethanamine [14] and ammonium chloride [15,16]. The properties of N-doped TiO₂ have already been discussed with respect to the nitrogen content [8], the oxidative power [9], desorption of nitrogen from the O–Ti–O matrix during annealing [14], characterization of different prepared materials [15], increase of carrier-recombination centers in TiO₂ [11], and the effect of Fe₂O₃ nanoparticles on N-doped TiO₂ [12]. Irie et al. reported that increasing nitrogen concentrations in TiO_{2-x}N_x powders

with $x < 0.02$ resulted in decreasing quantum yields and suggested that the doping sites could also serve as recombination sites [7].

In general, phosphorous-doped (P-doped) TiO₂ prepared using phosphate is not able to absorb visible light. Several groups [21–24] have reported that P-doped TiO₂ prepared using H₃PO₄ exhibited a band gap slightly larger than that of pure TiO₂. On the other hand, the results of several studies on P-doped TiO₂ prepared using phosphate demonstrated band gap narrowing (a slight red shift of the absorption edge) [25–28]. In those studies, P-doped TiO₂ was synthesized by a sol–gel method where H₃PO₂ (P⁺) [25–27] or H₃PO₄ (P⁵⁺) [28] was used as a P precursor. The band-gap energies of P-doped TiO₂ prepared using H₃PO₂ and H₃PO₄ were 3.13 eV (absorption edge: 396 nm) [26] and 3.11 eV (399 nm) [28], respectively. Those studies suggested formation of Ti–O–P bonds in the anatase lattice [27,28]. The P species in the titania were considered to be the dominant group responsive to the small change in band gap [27].

We have reported the characterization of P-doped TiO₂ prepared by calcination after grinding phosphide (P³⁻) and TiO₂ materials in a mortar [29]. However, a shift of the absorption edge was not apparent. In another study, we synthesized P-doped TiO₂ particles by hydrolysis of titanium tetraisopropoxide in a suspension containing phosphide [30]. The product P-doped TiO₂ nanoparticles were found to exhibit a pale yellow color. The action spectra of the photocatalytic decomposition of acetaldehyde

* Corresponding author. Tel.: +81 92 801 8883; fax: +81 92 801 8883.

E-mail address: wakita@fukuoka-u.ac.jp (H. Wakita).

revealed visible-light activity of the P-doped TiO₂ particles. P-doped TiO₂ particles calcined at 475 °C exhibited the highest rate of phenol degradation in visible light. We succeeded in, for the first time, the synthesis of P-doped TiO₂ with a red shift of the absorption edge and visible-light photocatalytic activity using a phosphide compound as P precursor. When the P/Ti ratio was in the range of 0.01–0.02, the absorption edges of our sample and of P-doped TiO₂ prepared using H₃PO₄ (P⁵⁺) [28] and H₃PO₂ (P³⁺) [26] were 422, 399 and 396 nm, respectively. The trend was consistent with theoretical predictions [31], indicating that the band gap of the doped TiO₂ was narrowed for P anion-doped TiO₂ (anatase) prepared by replacement of lattice O²⁻ by P³⁻ and little narrowed for P cation-doped TiO₂ prepared by replacement of lattice Ti⁴⁺ by P⁵⁺.

The purpose of the present study is to investigate phosphorus-concentration dependence of properties of P-doped TiO₂ prepared using phosphide (P³⁻). Correlations between the density of oxygen vacancies and the visible-light photocatalytic activity of the P-doped TiO₂ particles are discussed.

2. Experimental

2.1. Preparation of P-doped TiO₂ particles

All chemicals used in this study were purchased from Wako Pure Chemical Industries, Ltd. unless otherwise noted.

P-doped TiO₂ (P-TiO₂) particles were synthesized by calcination of the precipitates from the hydrolysis of titanium tetraisopropoxide in a suspension containing phosphide. First, phosphide was synthesized as follows: titanium tetrachloride was mixed with two molar equivalents of cyclohexylphosphine (Strem Chemicals Inc.) in hexane at ambient temperature. [TiCl₄(C₆H₁₁PH₂)₂] was isolated as a yellow solid by filtration [32]. After the yellow solid had been heated in an ampoule under nitrogen atmosphere at 450 °C for 6 h, a black solid (denoted as *TiP compound*) was obtained. Then the phosphide and TiO₂ materials were combined by dispersion of the *TiP compound* in a mixture of 2.84 g titanium tetraisopropoxide and 6 mL 2-propanol. Hydrolysis of the product was achieved by adding 30 mL of deionized water (Milli-Q water, Millipore) to the mixture dropwise with stirring. A gray precipitate was produced instantly, and the mixture was stirred for 10 min. The precipitate was separated by filtration and washed three times with deionized water. The collected solid was dried at 110 °C for 3 h and calcined at 500 °C for 6 h. The final products are denoted as P_x-TiO₂, where $x = \text{TiP compound}/\text{TiO}_2$ materials (mass ratio). ST01 (Ishihara Sangyo Kaisha, Ltd., Japan) was used as a reference. Pure TiO₂ was prepared in the same way with the exception of the addition of *TiP compound*. PO₄-adsorbed TiO₂ was prepared as follows: ST01 powder (1.0 g) was added to 100 mL aqueous H₃PO₄ solution (20 mM), and the solution was stirred for 1 h in the dark. The resulting PO₄-adsorbed TiO₂ powder was filtered and dried at 110 °C for 3 h.

2.2. Characterization

The crystal structure of TiO₂ was examined by X-ray diffraction (XRD) using a Rigaku Multiflex 2 kW instrument with a Cu-K_α source. IR spectra were obtained using a JASCO FT/IR-480Plus spectrometer. UV–vis absorption spectra were recorded with a JASCO V-570 UV–vis spectrometer. ESR spectra were recorded at room temperature on a JEOL JES-FA200 Electron Spin Resonance Spectrometer at a microwave frequency of 9.43 GHz, a microwave power of 2 mW and a modulation frequency of 100 kHz. The chemical composition of the surface of the TiO₂ was examined by X-ray photoelectron spectroscopy (XPS) using a PHI 1800 spectrometer equipped with a monochromatic Al-K_α source at a pass energy of

23.5 eV. The core level binding energies were aligned with respect to the C 1s binding energy of 285 eV. An electron flood gun was used to compensate for the build-up of positive charge on the insulated samples during the measurement. Ar⁺ sputtering (2 kV) was applied to clean the sample surfaces. The specific surface area of TiO₂ particles was analyzed by the BET method from N₂ adsorption isotherms at 77 K using a BELSORP-max instrument. Samples were dried at 110 °C for 3 h before the adsorption measurement.

2.3. Photocatalytic activity measurements

The photocatalytic activity of the P-TiO₂ particles was determined by measuring the degradation of phenol and the appearance of 1,4-benzoquinone under irradiation. Phenol is a model compound for photocatalytic degradation [33]. Irradiation was performed with a 450-W incandescent lamp (Iwasaki Electric Co. Ltd.). Emission wavelengths in the 423–600 nm range were selected using a Y-45 glass filter (AGC Techno Glass Co., Ltd.) and an aqueous nickel sulfate solution. An aqueous suspension (50.0 mL) of TiO₂ (1.00 g/L) and phenol (0.050 mM) was prepared and stirred for 15 min prior to and during the irradiation. After irradiation, samples were filtered by a 0.45 μm filter (Sartorius, MINISART RC4) for analysis by HPLC (Shiseido Fine Chemicals, Nanospace System) equipped with a reverse-phase column (Shiseido Fine Chemicals, C18AQ) with an H₃PO₄ buffer (0.1 wt%)/CH₃OH (90:10) solution. Quantification of phenol and degradation products was performed using a photodiode-array detector at 260 nm.

2.4. Action spectra

Action spectra were measured by irradiation with monochromatic light irradiation at 410, 440 and 470 nm using a diffraction grating-type illuminator (JASCO, CRM-FD) equipped with a 300 W xenon lamp (Hamamatsu Photonics, C2578-02). The light intensity at each wavelength was measured with a power meter (HIOKI 3664). Full-width at half-maximum intensity (FWHM) of the monochromatic light was ca. 15 nm. A container containing the sample photocatalyst (10 mg) fixed on a glass plate and acetaldehyde was sealed and kept in the dark for 2 h to reach an adsorption equilibrium. The molar amount of CO₂ liberated by photocatalytic decomposition of acetaldehyde was measured by a gas chromatograph (Shimadzu, GC-14B) equipped with an FID and a methanizer (Shimadzu, MTN-1).

3. Results and discussion

3.1. Photocatalyst structure

Fig. 1 shows XRD patterns of P-TiO₂ and ST01. The XRD patterns of the P-TiO₂ particles correspond to the pattern of ST01 which is in the anatase form. A small peak at approximately 31° indicates the existence of a small quantity of brookite crystallites. This is consistent with the results of a study [34] in which sol–gel synthesis of titania was found to produce a mixture of brookite and anatase. Crystallite size, D , was determined using Scherrer's equation [35]:

$$D = \frac{0.89\lambda}{\beta \cos \theta} \quad (1)$$

where λ (nm) is the X-ray wavelength, θ is the Bragg angle, and β is the corrected full width at half maximum (FWHM) of the most intense diffraction peak. The crystallite sizes of P-TiO₂ samples and of ST01 are summarized in Table 1. The size of ST01 was 8.3 nm, comparable to previously-reported crystallite size [36]. The crystallite size of the P-TiO₂ samples was found to decrease with increasing phosphorus concentration. The specific surface areas of P-TiO₂ and ST01 are also summarized in Table 1. The surface area

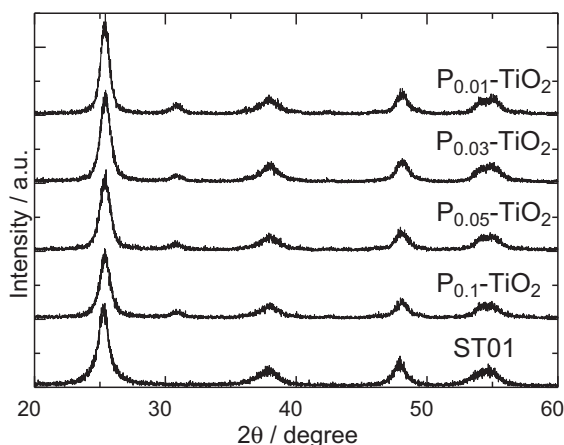


Fig. 1. XRD patterns of ST01 and P-TiO₂ with varying P concentration.

Table 1

Crystallite sizes and surface areas of P-TiO₂, pure TiO₂ and ST01.

Sample	Crystallite size (nm)	Surface area (m ² g ⁻¹)
ST01	8.3	297
Pure TiO ₂	17	39
P _{0.01} -TiO ₂	11	89
P _{0.03} -TiO ₂	10	101
P _{0.05} -TiO ₂	9.0	110
P _{0.1} -TiO ₂	8.7	115
P _{0.2} -TiO ₂	6.8	132

of ST01 is in good agreement with previously-reported data [36]. The surface area of the P-TiO₂ particles was found to increase with increasing phosphorus concentration as expected from the results of crystallite size. These results indicate that P atom dopants inhibit crystalline growth.

3.2. FTIR spectra

Fig. 2 shows FTIR spectra of P-TiO₂ and pure TiO₂. The peaks observed in the range of 700–1250 cm⁻¹ are characteristic of formation of the O–Ti–O lattice [15]. The infrared spectra of all samples show peaks at 1630 cm⁻¹, 2340 cm⁻¹ and 3400 cm⁻¹ (broad), which are ascribed to OH groups [15], adsorbed CO₂ [16] and residual adsorbed water [16], respectively. The intensities of the 1630 cm⁻¹ and 3400 cm⁻¹ peaks decrease with increasing P concentration. A small peak at 1100 cm⁻¹ was

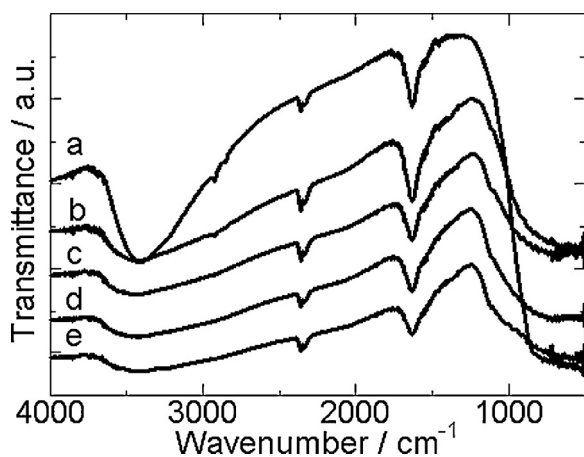


Fig. 2. IR spectra of (a) pure TiO₂, (b) P_{0.01}-TiO₂, (c) P_{0.03}-TiO₂, (d) P_{0.05}-TiO₂, and (e) P_{0.1}-TiO₂.

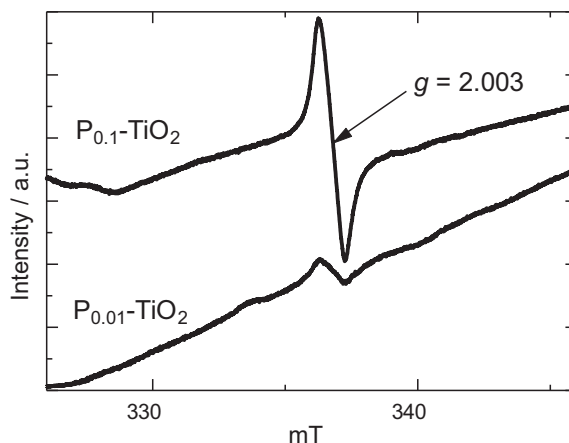


Fig. 3. ESR spectra of P_{0.01}-TiO₂ and P_{0.1}-TiO₂.

observed in the spectra of the P-TiO₂ particles. The 1100 cm⁻¹ peak was well accorded with the peak of PO₄ on the surface of PO₄-doped TiO₂ that absorbed only UV light [37]. This observation suggests partial oxidation of P on the surface of TiO₂ in our calcination process. A peak around 1300 cm⁻¹, which would be characteristic of the presence of C–H bonds [14], was not detected. Zhao et al. reported that the IR signals for the organic groups of the raw material disappeared after heating the samples at 400 °C for 30 min [13]. Because the P-TiO₂ samples were calcined at 500 °C for 6 h, no peak corresponding to hydrocarbon is present in their spectra.

3.3. ESR spectra

Fig. 3 shows ESR spectra of two P-TiO₂ particles measured at room temperature in air. The ESR spectrum of pure TiO₂ shows no signal, which indicates an absence of paramagnetic species (not shown). The *g*-factor (*g* = 2.003) of the P-TiO₂ particles was close to that of free electron. The symmetrical signals of the P-TiO₂ particles are assigned to single-electron-trapped oxygen vacancies (SETOV) [38]. Since the intensity of ESR signal is proportional to the concentration of paramagnetic species, the amount of oxygen vacancies observed in P_{0.1}-TiO₂ was approximately 6 times greater than that in P_{0.01}-TiO₂. During the preparation of the P-TiO₂ particles, the replacement of O²⁻ by P³⁻ produces oxygen vacancies. In order to maintain the overall electroneutrality of the crystal lattice, incorporation of two P atoms into the oxygen sites causes formation of one oxygen vacancy. Due to this phenomenon, a high P content in the lattice may lead to a large number of oxygen vacancies.

3.4. UV-vis absorption spectra

Fig. 4 shows absorption spectra of P-TiO₂ and pure TiO₂. All of the synthesized P-TiO₂ samples exhibit a pale yellow color. The absorption edge of approximately 400 nm for pure TiO₂ can be assigned to electronic transitions from the valance band to the conduction band for the anatase phase. The spectra of the P-TiO₂ particles, which contain both the anatase and brookite form, clearly exhibit a red-shifted onset and broad absorption in the visible region. The red shift of the P-TiO₂ particles is not attributable to brookite phase since the band-gap energy of brookite has been reported as 3.14 eV [39]. The intensity of the broad absorption in the range of 500–600 nm increased with increasing P content. Hydrogen-reduced TiO₂ powders were known as an example of TiO₂ particles having a large quantity of oxygen vacancies [7]. The powder exhibited a gray color, which indicates absorption over the entire range of visible light. The results of the previous study suggest that the increase of broad absorption in the range of 500–600 nm in Fig. 4

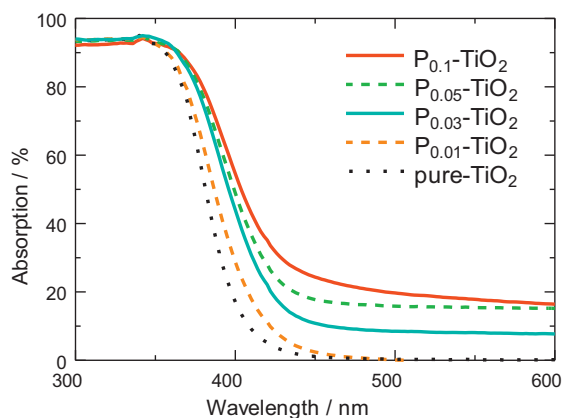


Fig. 4. Absorption spectra of pure TiO₂ and P-TiO₂ with varying P concentration.

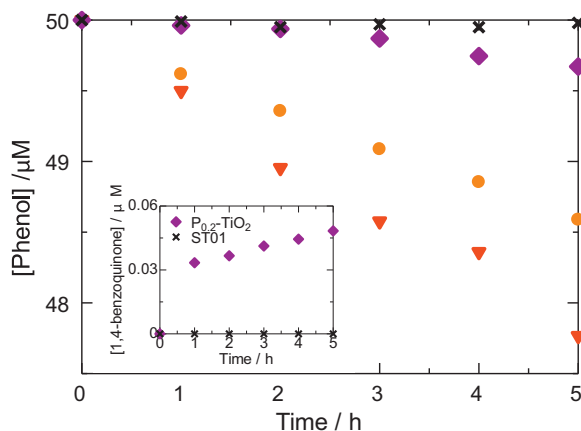


Fig. 5. Phenol degradation on P_{0.01}-TiO₂ (●); P_{0.1}-TiO₂ (▼); P_{0.2}-TiO₂ (◆) and ST01 (×) under visible-light irradiation as a function of irradiation time. (Insert) 1,4-benzoquinone formation on P_{0.2}-TiO₂ (◆) and ST01 (×) under visible-light irradiation as a function of irradiation time.

is due to an increase in oxygen vacancies. Thus, P-TiO₂ particles exhibit two types of visible-light absorption bands at 400–450 nm and >500 nm.

3.5. Photocatalytic phenol degradation

Fig. 5 shows phenol degradation and 1,4-benzoquinone formation on P-TiO₂ and ST01 under visible-light irradiation (423–600 nm) as a function of irradiation time. Phenol degradation along with 1,4-benzoquinone liberation was observed for P-TiO₂ samples but not for ST01. The phenol degradation and 1,4-benzoquinone appearance in the case of P-TiO₂ particles indicate visible light activity of P-TiO₂ particles. Table 2 shows apparent pseudo-first-order rate constants k_{app} for the photodegradation of phenol in the presence of P-TiO₂ particles. Up to $x = 0.1$ in P_x-TiO₂, k_{app} increases with increasing P content. On the other hand, k_{app}

Table 2
Apparent rate constants k_{app} for phenol photodegradation in the presence of P-TiO₂ and ST01 under visible light irradiation.

Sample	k_{app} (h ⁻¹)
ST01	0
P _{0.01} -TiO ₂	0.0061
P _{0.03} -TiO ₂	0.0066
P _{0.05} -TiO ₂	0.0086
P _{0.1} -TiO ₂	0.0091
P _{0.2} -TiO ₂	0.0011

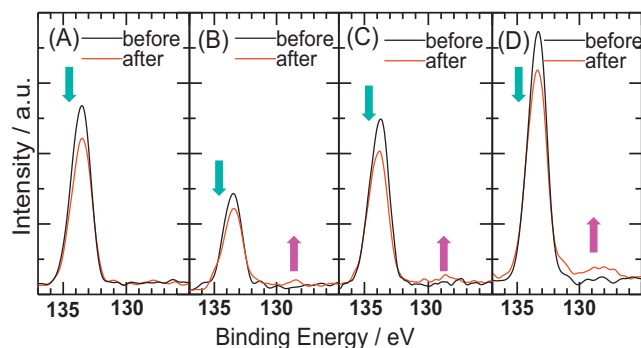


Fig. 6. XPS P2p spectra of PO₄-adsorbed TiO₂ (A) and P_{0.02}-TiO₂ (B), P_{0.05}-TiO₂ (C) and P_{0.1}-TiO₂ (D) before and after Ar⁺ sputtering.

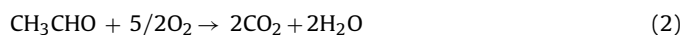
decreases with increasing the ratio of P above $x = 0.1$. Figs. 3 and 4 show that oxygen vacancies remarkably increased with increasing P content from 0.01 to 0.1. However, the difference of k_{app} between P_{0.01}-TiO₂ and P_{0.1}-TiO₂ was small. These results indicate that the oxygen vacancies in P-TiO₂ particles are inactive to visible light, as has been reported previously as hydrogen-reduced TiO₂ powders with a large quantity of oxygen vacancies were not visible-light sensitive [7]. A previous study claimed that high specific surface area is related to high photocatalytic efficiency [40] because a high specific surface area allows the adsorption of a greater amount of organic compounds (phenol). For the samples used in the present study, the specific surface area increased with increasing P content as shown in Table 1. This characteristic may enhance the photocatalytic efficiency as discussed above. On the other hand, the oxygen vacancy produced by P doping is thought to act as a recombination center for holes and electrons since the oxygen vacancy state in anatase TiO₂ is below the bottom of the conduction band at 0.75–1.18 eV [41]. The relatively low photocatalytic activity of P_{0.2}-TiO₂ can be attributed to enhanced recombination by oxygen vacancies negating enhanced visible-light photoabsorption and high specific surface area.

3.6. XPS analysis

Fig. 6 shows P 2p spectra of P-TiO₂ and PO₄-adsorbed TiO₂ before and after Ar⁺ sputtering. Only a peak at 134 eV was observed for PO₄-adsorbed TiO₂, which can be assigned to P⁵⁺ [22], the most likely in the form of phosphate. An increase of the peak intensity at 134 eV for the P-TiO₂ samples with increasing P content indicates an increase in phosphate content. Another peak at approximately 128 eV is assigned to P³⁻ [22]. The intensities of the peak at 128 eV for P-TiO₂ after sputtering increased with increasing P content. The decrease of P⁵⁺ and the increase of P³⁻ during sputtering suggest the presence of phosphate on the surface and the presence of P³⁻ in the bulk of P-doped TiO₂; the partial oxidation of phosphide during our synthetic process could result in formation of phosphate on the surface of P-TiO₂ particles. A theoretical calculation [31] predicted that visible-light absorption by P-TiO₂ particles would require the replacement of O atoms by P atoms having negative charges in the TiO₂ anatase matrix. The red shift of the absorption edge of the P-TiO₂ particles is interpreted as band gap narrowing induced by P³⁻ atoms in the TiO₂ anatase matrix.

3.7. Action spectra of acetaldehyde degradation

Action spectra were analyzed in order to clarify the origin of visible-light photocatalytic activity. Fig. 7(A) shows the action spectra of photocatalytic decomposition of acetaldehyde.



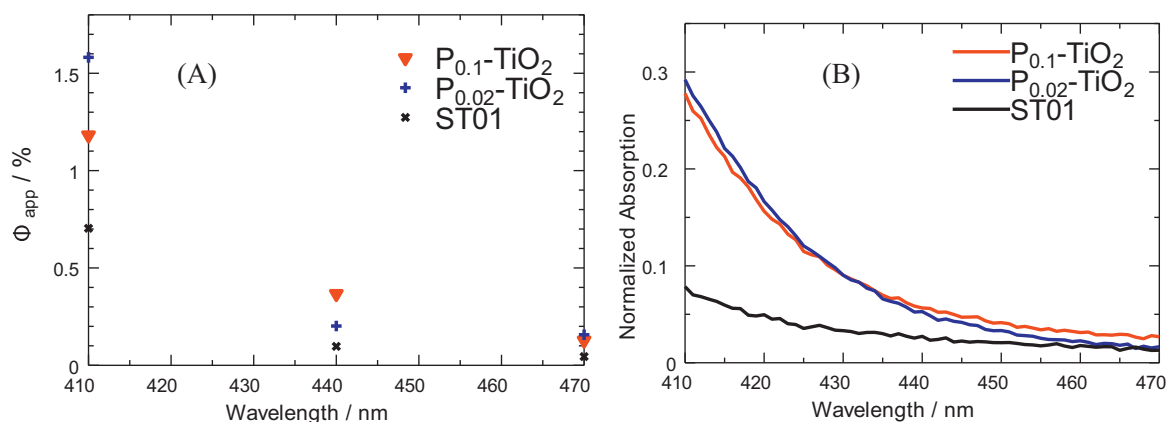


Fig. 7. (A) Action spectra and (B) normalized absorption spectra of P-TiO₂ and ST01.

The apparent quantum efficiency Φ_{app} was calculated as a ratio of the molar rate of the CO₂ generation to the flux of incident photons by assuming the formation of a CO₂ molecule with five electron–hole pairs [42–44]. Since apparent quantum efficiency is a product of the efficiencies of photoabsorption and electron–positive hole utilization [44], an action spectrum reflects the photoabsorption of species inducing the photoreaction. The action spectra of the P-TiO₂ particles corresponded well to the absorption spectra in our previous report [30], and the apparent quantum efficiency of acetaldehyde decomposition by the P-TiO₂ particles was found to depend mainly on the efficiency of photoabsorption. The appreciable apparent quantum efficiencies of P-TiO₂ and ST01 in the 410–470 nm wavelength range revealed the visible light photocatalytic activity of P-TiO₂ particles. ST01 exhibited negligible absorption at 410 nm but relatively high apparent quantum efficiency. This is likely due to the relatively large FWHM of the monochromatic light used in these experiments; the monochromatic light at 410 nm contained ultraviolet light, which is able to excite anatase TiO₂. This explanation is consistent with the negligible apparent quantum efficiency of ST01 at 440 nm. The apparent quantum efficiency of P_{0.1}-TiO₂ at 470 nm was almost the same as that of P_{0.02}-TiO₂, even though the absorption at the wavelength of P_{0.1}-TiO₂ shown in Fig. 4 was much higher, suggesting that the broad absorption band observed at longer wavelengths that was assigned to oxygen vacancies does not contribute to the visible-light photocatalysis. P-TiO₂ particles exhibit two types of visible-light absorption bands at 400–450 nm originating from P³⁻ atoms in the anatase matrix and >500 nm derived from oxygen vacancies. Thus, the photocatalytic activity under visible light of P-TiO₂ is due to P³⁻ atoms in the anatase matrix. Absorption spectra (Fig. 7(B)) normalized in the range of 300–550 nm represent the absorption spectra after subtraction of broad-band absorption that was attributed to the oxygen vacancies. The absorption of P_{0.1}-TiO₂ was lower at 410 nm and higher at 440 nm than that of P_{0.02}-TiO₂. The trend observed here corresponds to the observation made on the action spectra. These results indicate that the spectral shape of the absorption due to the formation of visible-light active sites by P atom dopants may depend on the P concentration in P-TiO₂ particles.

4. Conclusions

The properties of P-doped TiO₂ particles with varying concentrations of negatively-charged phosphorus were investigated. The increase in P concentration led to a decrease of crystallite size and an increase of specific surface area. These results indicate that P atom dopants inhibit crystalline growth. Increasing P content also resulted in a marked increase of the broad absorption in the

range of 500–600 nm assignable to oxygen vacancies in the matrix of the particles. The small difference in rate constants of phenol degradation under visible-light irradiation between P_{0.01}-TiO₂ and P_{0.1}-TiO₂ indicates that oxygen vacancies in P-TiO₂ particles are inactive to visible light. Comparison of the action spectra and the normalized absorption spectra of the particles suggests that the shape of the absorption spectrum resulting from the formation of visible-light active sites by P atom dopants may depend on the P concentration in P-TiO₂. These results indicate that P³⁻-doped TiO₂ requires further study as a novel nonmetal-doped TiO₂ material with visible-light photocatalytic activity.

Acknowledgments

The authors thank Dr. Kosei Shioji for the use of his visible-light lamp, Prof. Satoshi Kawata for the XRD measurement, Dr. Yoshio Murata for the use of the reflectance spectrometer and Prof. Toshio Yamaguchi for assistance in surface area analysis and IR experiments. Dr. Shioji, Prof. Kawata, Dr. Murata and Prof. Yamaguchi are all affiliated with Fukuoka University. The authors thank Dr. Yoshihiro Okaue of Kyushu University for the use of the Electron Spin Resonance Spectrometer. This study was supported by the Cooperative Research Program of Catalysis Research Center, Hokkaido University (Grant #11B2005). This work was partly supported by Grant-in-Aid for Scientific Research (B) (20350040) and (C) (22550088).

References

- [1] M.R. Hoffmann, S.T. Martin, W.Y. Choi, D.W. Bahnemann, *Chemical Reviews* 95 (1995) 69–96.
- [2] T.L. Thompson, J.T. Yates Jr., *Chemical Reviews* 106 (2006) 4428–4453.
- [3] B. Ohtani, *Journal of Photochemistry and Photobiology C: Photochemistry Reviews* 11 (2010) 157–178.
- [4] M. Anpo, Y. Ichihashi, M. Takeuchi, H. Yamashita, *Research on Chemical Intermediates* 24 (1998) 143–149.
- [5] A. Zielinska, E. Kowalska, J.W. Sobczak, I. Lacka, M. Gazda, B. Ohtani, J. Hupka, A. Zaleska, *Separation and Purification Technology* 72 (2010) 309–318.
- [6] R. Asahi, T. Morikawa, T. Ohwaki, K. Aoki, Y. Taga, *Science* 293 (2001) 269–271.
- [7] H. Irie, Y. Watanabe, K. Hashimoto, *Journal of Physical Chemistry B* 107 (2003) 5483–5486.
- [8] T. Matsumoto, Y. Hashimoto, M. Sakai, W. Shimizu, T. Nishikawa, Y. Murakami, N. Iyi, B. Ohtani, *Topics in Catalysis* 52 (2009) 1584–1591.
- [9] M. Mrowetz, W. Balcerski, A.J. Colussi, M.R. Hoffmann, *Journal of Physical Chemistry B* 108 (2004) 17269–17273.
- [10] E.A. Reyes-Garcia, Y. Sun, K. Reyes-Gil, D. Raftery, *Journal of Physical Chemistry C* 111 (2007) 2738–2748.
- [11] F. Amano, R. Abe, B. Ohtani, *Transactions of the Materials Research Society of Japan* 33 (2008) 173–176.
- [12] K. Nishijima, B. Ohtani, X. Yan, T. Kamai, T. Chiyoda, T. Tsubota, N. Murakami, T. Ohno, *Chemical Physics* 339 (2007) 64–72.
- [13] Y. Zhao, X. Qiu, C. Burda, *Chemistry of Materials* 20 (2008) 2629–2636.

- [14] T.C. Jagadale, S.P. Takale, R.S. Sonawane, H.M. Joshi, S.I. Patil, B.B. Kale, S.B. Ogale, *Journal of Physical Chemistry C* 112 (2008) 14595–14602.
- [15] S. Livraghi, M.R. Chierotti, E. Giamello, G. Magnacca, M.C. Paganini, G. Cappelletti, C.L. Bianchi, *Journal of Physical Chemistry C* 112 (2008) 17244–17252.
- [16] C.D. Valentin, G. Pacchioni, A. Selloni, S. Livraghi, E. Giamello, *Journal of Physical Chemistry B* 109 (2005) 11414–11419.
- [17] S.U.M. Khan, M. Al-Shahry, W.B. Ingler Jr., *Science* 297 (2002) 2243–2245.
- [18] B. Neumann, P. Bogdanoff, H. Tributsch, S. Sakthivel, H. Kisch, *Journal of Physical Chemistry B* 109 (2005) 16579–16586.
- [19] Y. Izumi, T. Itoi, S. Peng, K. Oka, Y. Shibata, *Journal of Physical Chemistry C* 113 (2009) 6706–6718.
- [20] X. Tang, D. Li, *Journal of Physical Chemistry C* 112 (2008) 5405–5409.
- [21] L. Korosi, I. Dekany, *Engineering Aspects* 280 (2006) 146–154.
- [22] J.C. Yu, L. Zhang, Z. Zheng, J. Zhao, *Chemistry of Materials* 15 (2003) 2280–2286.
- [23] Y. Lv, L. Yu, H. Huang, H. Liu, Y. Feng, *Journal of Alloys and Compounds* 488 (2009) 314–319.
- [24] L. Korosi, S. Papp, I. Bertoti, I. Dekany, *Chemistry of Materials* 19 (2007) 4811–4819.
- [25] L. Lin, Y. Zhu, B. Zhao, Y. Xie, *Chemistry Letters* 34 (2005) 284–285.
- [26] L. Lin, W. Lin, J.L. Xie, Y.X. Zhu, B.Y. Zhao, Y.C. Xie, *Applied Catalysis B* 75 (2007) 52–58.
- [27] R. Zheng, L. Lin, J. Xie, Y. Zhu, Y. Xie, *Journal of Physical Chemistry C* 112 (2008) 15502–15509.
- [28] F. Li, Y. Jiang, M. Xia, M. Sun, B. Xue, D. Lin, X. Zhang, *Journal of Physical Chemistry C* 113 (2009) 18134–18141.
- [29] M. Iwase, Y. Fujio, S. Nagahama, K. Yamada, T. Kurisaki, H. Wakita, *Advances in X-ray Chemical Analysis, Japan* 42 (2011) 213–219.
- [30] M. Iwase, K. Yamada, T. Kurisaki, O.O. Prieto-Mahaney, B. Ohtani, H. Wakita, *Applied Catalysis B: Environmental* 132/133 (2013) 39–44.
- [31] K. Yang, Y. Dai, B. Huang, *Journal of Physical Chemistry C* 111 (2007) 18985–18994.
- [32] T.S. Lewkebandara, J.W. Proscia, C.H. Winter, *Chemistry of Materials* 7 (1995) 1053–1054.
- [33] S.T. Martin, C.L. Morrison, M.R. Hoffmann, *Journal of Physical Chemistry* 98 (1994) 13695–13704.
- [34] S.L. Isley, R.L. Penn, *Journal of Physical Chemistry B* 110 (2006) 15134–15139.
- [35] H.P. Klug, L.E. Alexander, *X-ray Diffraction Procedure*, John Wiley & Sons Inc., New York, 1954.
- [36] Y. Nosaka, M. Matsushita, J. Nishino, A.Y. Nosaka, *Science and Technology of Advanced Materials* 6 (2005) 143–148.
- [37] Y. Arai, D.L. Sparks, *Journal of Colloid and Interface Science* 241 (2001) 317–326.
- [38] A. Kachina, E. Puzenat, S. Ould-Chikh, C. Geantet, P. Delichere, P. Afanasiev, *Chemistry of Materials* 24 (2012) 636–642.
- [39] M. Graetel, F. Rotzinger, *Chemical Physics Letters* 118 (1985) 474–477.
- [40] G. Tian, H. Fu, L. Jing, B. Xin, K. Pan, *Journal of Physical Chemistry C* 112 (2008) 3083–3089.
- [41] I. Nakamura, N. Negishi, S. Katsuna, T. Ihara, S. Sugihara, K. Takeuchi, *Journal of Molecular Catalysis A: Chemical* 161 (2000) 205–212.
- [42] T. Torimoto, Y. Aburakawa, Y. Kawahara, S. Ikeda, B. Ohtani, *Chemical Physics Letters* 392 (2004) 220–224.
- [43] B. Ohtani, *Chemistry Letters* 37 (2008) 217–229.
- [44] M.V. Dozzi, B. Ohtani, E. Selli, *Physical Chemistry Chemical Physics* 13 (2011) 18217–18227.